CrossMark

ORIGINAL PAPER

One-step electrodeposition of polyaniline/nickel hexacyanoferrate/sulfonated carbon nanotubes interconnected composite films for supercapacitor

Yonghong Wang[1] · Yujiao Yang[1] · Xinru Zhang[1] · Chengcen Liu[1] · Xiaogang Hao[1]

Abstract Sulfonated carbon nanotubes (sCNTs) were prepared by reacting concentrated sulfuric acid with carbon nanotubes (CNTs) on the defect sites. Fourier transform infrared (FTIR) spectroscopy and transmission electron microscopy (TEM) were used to characterize the morphology and structure of sCNTs, respectively. Subsequently, polyaniline (PANI)/nickel hexacyanoferrate (NiHCF)/sCNT interconnected composite films were electrodeposited on the platinum electrode by the one-step co-polymerization using cyclic voltammetry in an aqueous dispersion containing sCNTs. The effect of concentration of $NiSO_4$ and $K_3Fe(CN)_6$ in the prepared solution on the morphology and structure of PANI/NiHCF/sCNTs composite films was studied by scanning electron microscopy (SEM), FTIR spectroscopy, and X-ray diffraction (XRD), respectively. The effect of concentration of $NiSO_4$ and $K_3Fe(CN)_6$ in the prepared solution on polymerization and electrochemical performance was investigated by cyclic voltammetry (CV), galvanostatic charge/ discharge tests, and electrochemical impedance spectroscopy (EIS). One-step electrodeposition mechanism was discussed deeply. It was found that sulfonic acid groups had been attached to surface of CNTs, and sCNTs had higher dispersibility than CNTs in an aqueous dispersion. The morphology of PANI/NiHCF/sCNTs interconnected composite films was remarkably influenced by the concentration of $NiSO_4$ and $K_3Fe(CN)_6$. The tubular packing structure appeared with the low concentration of $NiSO_4$ and $K_3Fe(CN)_6$ in prepared solution, while the beautiful coral-like interconnected structure exhibited with 0.04 mol L^{-1} $NiSO_4$ and 0.04 mol L^{-1} $K_3Fe(CN)_6$, which was mainly attributed to the π–π* electron stacking effect among sCNTs, NiHCF, and PANI. The specific capacitance and electroactivity of PANI/NiHCF/sCNTs composite films increased markedly with the increase of concentration of $NiSO_4$ and $K_3Fe(CN)_6$ in prepared solution. The specific capacitance of PANI/NiHCF/sCNTs composite film was 430.77 F g^{-1} with 0.04 mol L^{-1} $NiSO_4$ and 0.04 mol L^{-1} $K_3Fe(CN)_6$ due to self-doping effect of sCNT in composite films. The cycle stability of PANI/NiHCF/sCNTs composite films was enhanced with the increase of $NiSO_4$ and $K_3Fe(CN)_6$ in prepared solution.

Keywords Carbon nanotubes · Polyaniline · Composite films · One-step electrodeposition · Supercapacitive performance

Introduction

Supercapacitor is thought as one of potential storage energy device due to its wide range of potential applications, such as hybrid power sources for electric vehicles, digital telecommunication systems, and pulse laser technique, especially for environment-friendly car [1–4]. They possess higher power density, longer cycle life and higher energy density than secondary batteries. According to the mechanism of energy storage, supercapacitor can be divided into two types [5]: the electrochemical double-layer capacitor [6] can store energy through the separation of electronic and ionic charges at the interface between electrode and electrolyte solution; the other is pseudocapacitor [7], which has Faradic reactions on the electrode as a result of redox reaction of electroactive materials. The electrode materials of supercapacitors are mainly

✉ Xinru Zhang
zhangxinru@tyut.edu.cn

[1] Department of Chemical Engineering, Taiyuan University of Technology, Taiyuan 030024, China

made from high-surface carbons, transition metal oxides, and conducting polymers [8].

Carbon materials present electric double-layer capacitor mainly derived from positive and negative charge accumulation on the electrode surface, which has smaller distance and larger specific area than conventional capacitor [9]. However, the energy density of carbon materials was low in comparison with pseudocapacitor. The energy density of pseudocapacitor made from conducting polymers and transition metal oxides is 10–100 times as high as that of electric double-layer capacitor, but this kind of electrode materials possesses low conductivity and cyclic life [10]. In order to enhance the electrochemical properties and create synergistic effect by combining the advantages of electric double-layer capacitor with faradaic pseudocapacitor [11], carbon/conducting polymers/transition metal oxide composite materials have been paid much attention [12].

Polyaniline (PANI) is a popular candidate for practical applications in supercapacitors due to its good processability, environmental stability, low cost, and reversible control of electrical properties by both charge-transfer doping and protonation [13, 14]. Carbon nanotubes (CNTs) have been regarded as excellent filler for polymer in improving the electric conductivity as well as the mechanical properties for application in supercapacitors [15, 16]. Nickel hexacyanoferrate (NiHCF) is an inorganic coordination compound with an open, zeolite-like structure and redox-active Fe(II/III) centers bound to Ni(II) cations via cyanide bridges, which possesses high supercapacitive performances and cycling stability [17, 18]. PANI composites with CNTs and NiHCF have been received much more attention of researchers due to high electrocatalytic, ion-exchange, and supercapacitive properties. Also, it has been demonstrated that the obtained composites possess the properties of each of the constituents with a synergistic effect.

Many groups had contributed to preparation of PANI/NiHCF/CNTs composite films and achieved the outstanding results. Lin et al. [19] synthesized the PANI/NiHCF/CNTs composite films by step-by-step electrodeposition on glassy carbon electrodes with CNTs. It was found that the nanocomposite films had good ion exchange capacity, high stability, and selectivity for caesium ions. Our group [20–22] also synthesized PANI/NiHCF/CNTs composite films on platinum substrates with CNTs using cyclic voltammetry and pulse potentiostatic method. The specific capacitance of composite films was 262.28 F g^{-1} with a specific energy of 29.51 Wh kg^{-1} at a current density of 2 mA cm^{-2}. The sensitivity of composites films for hydrogen peroxide detection is 3119 mA M^{-1} cm^{-2}, and the detection concentration range is from 1.25×10^{-6} to 2.95×10^{-3} M. The results showed that composites films have outstanding power performance, fast dynamics of charge transport, electrocatalytic property, and were excellent materials for use in

supercapacitors and biosensors. However, the electrodeposition method of PANI/NiHCF/CNTs composite films was very complex, in which CNTs need to be coated on working electrode before electrodeposition. Also, CNTs could not be dispersed in the matrix uniformly due to insolubility, poor dispersibility, and bad compatibility, so CNTs had not significant effects to improve the electrochemical properties of composite films. To our knowledge, few reports have been discussed in the literature about PANI/NiHCF/sulfonated carbon nanotubes (sCNTs) composite films, which were electrodeposited in the three homogeneous compositions by one step directly.

The goal of our work is to make CNTs dispersed in PANI/NiHCF/CNTs composite films uniformly and achieve high supercapacitive properties. PANI/NiHCF/sCNTs composite films were deposited on the platinum electrode by one-step co-polymerization using cyclic voltammetry in the solution of sCNTs, NiSO$_4$, K$_3$Fe(CN)$_6$, and aniline. The effect of concentration of NiSO$_4$ and K$_3$Fe(CN)$_6$ on the polymerization, morphology, structure, and electrochemical performance of PANI/NiHCF/sCNTs composite films was investigated by cyclic voltammetry (CV), scanning electron microscopy (SEM), Fourier transform infrared (FTIR) spectroscopy, X-ray diffraction (XRD), galvanostatic charge/discharge tests, and electrochemical impedance spectroscopy (EIS), respectively. One-step co-polymerization mechanism was discussed in detail.

Experimental

Materials

Carbon nanotubes (CNTs) were obtained from Institute Process of Engineering, Chinese Academy of Science (Beijing, China). Aniline, nitric acid (70 wt.%) and sulfuric acid (98 wt.%) were supplied by Shanghai Chemical Reagent Co. (Shanghai, China). Aniline was distilled under vacuum prior to use and stored under high purified nitrogen, and other reagents were used as received without further treatment.

Preparation of sCNTs

Sulfonated carbon nanotubes with a high density of sulfonic acid groups were prepared by reacting sulfuric acid with carbon nanotubes on the defect sites. The typical procedures of sulfonation modification to CNTs was as follows [23–25]: 5 g of CNTs were suspended by a mixture of concentrated sulfuric acid (120 ml, 98 wt.%) and nitric acid (40 ml, 70 wt.%) solution and then ultrasonicated for a period of 2 h. The suspension was reacted in reflux condensers at 134 °C for 1 h, and then was cooled to room temperature. Subsequently, the resulting suspension was filtered, washed thoroughly with

deionized water for several times until no residual acid was present (pH >6). Finally, the filter sample was dried in a vacuum oven at 60 °C. The sample was abbreviated as sCNTs.

Electrode pretreatment

Platinum sheets (effective surface area, 0.5 cm^2) were polished carefully with alumina powder on a soft polishing cloth. Prior to the electrodeposition, they were treated with cyclic scanning in the potential range of −0.675 to 1.675 V at a scan rate of 100 mV s^{-1} for 50 times in 1.0 mol L^{-1} H$_2$SO$_4$ solution until the cyclic voltammogram characteristic for a clean platinum electrode was obtained, followed by rinsing thoroughly with deionized water, and then drying in a vacuum oven.

Electrodeposition of PANI/NiHCF/sCNTs composite films

The electrochemical synthesis of PANI/NiHCF/sCNT composite films was carried out in a three-electrode system (platinum sheets electrode as working electrode, platinum wire as counter electrode, and standard saturated calomel electrode as reference electrode) with VMP3 electrochemical workstation (Princeton, USA) controlled with EC-Lab software at room temperature. Thirty milligrams of sCNTs was suspended by the solution of 0.5 mol L^{-1} H$_2$SO$_4$; 0.25 mol L^{-1} Na$_2$SO$_4$; 0.005, 0.01, 0.02, and 0.04 mol L^{-1} NiSO$_4$; 0.005, 0.01, 0.02, and 0.04 mol L^{-1} K$_3$Fe(CN)$_6$; and 0.01 mol L^{-1} aniline, respectively. The electrochemical deposition experiments were carried out in the fresh suspension under quiescent conditions by CV method. The PANI/NiHCF/sCNT composite films were also fabricated by cycling the potential from −0.2 to 0.85 V at 0.05 V s^{-1} for 30 cycles. The composite films were washing with deionized water for several times until the films became acid free, and finally dried in vacuum oven at 60 °C for 12 h.

Characterization

The morphology of sCNTs was characterized by transmission electron microscopy (TEM, JEOL JEM-2010). The morphology of PANI/NiHCF/sCNTs composite films was investigated by scanning electron microscopy (SEM, JEOL JSM-6700F). FTIR spectroscopic measurements of the samples were recorded on a Japanese SHIMADZU FTIR-8400 spectrophotometer. The scanning wavenumber range of the experiment was 500–4000 cm^{-1} on transmittance mode with 30 scans at a resolution of 8.0 cm^{-1}. For each sample, three scans were taken to identify the peaks. The XRD spectra of composite films were taken in 5°–60° range at a scan rate of 8° min^{-1} using a Rigaku Miniflex II diffractometer (Japan) employing Cu-K$_a$ radiation, operating at 30 kV and 15 mA.

Electrochemical performance of composite films was performed by cyclic voltammeter (CV) from −0.2 to 0.85 V in 0.5 mol L^{-1} H$_2$SO$_4$ and 0.5 mol L^{-1} KNO$_3$ mixed solution. EIS was carried out with frequencies varying from 100 kHz to 0.1 Hz, using AC amplitude of 10 mV at open circuit potentials. Charge/discharge cycle tests were performed at different constant current densities, with cutoff voltage of 0 to 0.7 V. All electrochemical experiments were carried out with a conventional three-electrode system using VMP3 electrochemical workstation (Princeton, USA). The composite films were used as the working electrode. Platinum wire and standard saturated calomel electrode (SCE) were used as the counter electrode and the reference electrode, respectively. The mass of composite films was measured by a CPA225D electronic balance with a precision of ±0.01 mg (Sartorius, Germany).

Results and discussion

Structural characterization of sCNTs

Figure 1 shows the FTIR spectra of sCNTs and pristine CNTs, respectively. As shown in Fig. 1, the absorption peaks at 3442 cm^{-1} are assigned to –OH stretching vibration. The absorption peak at 1630 cm^{-1} is attributed to the C=C stretching vibration [26]. The absorption peak at 1374 cm^{-1} is corresponded to stretching vibration of the C–O–C, and the band at 1074 cm^{-1} is assigned to stretching vibration of the C–O [27]. The peak at 595 cm^{-1} is attributed to the deformation of C-H out of plane of aromatic ring. Compared to the pristine CNTs, some new absorption peaks appeared in the FTIR spectra of sCNTs. The strong band at 1720 cm^{-1} and the weak bands at 1460 and 1220 cm^{-1} are attributed to the stretching modes of sulfate groups [28, 29], which indicates the existence of the –SO$_3$H groups after sulfonation reaction. The
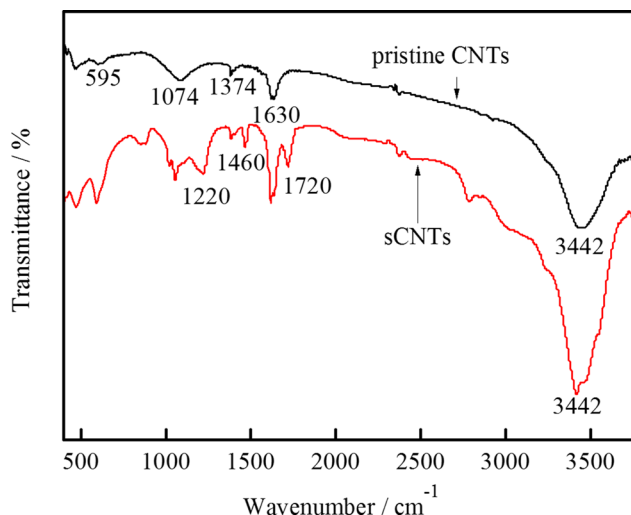

Fig. 1 FTIR spectra of sCNTs and pristine CNTs

intensity of absorption peak at 3442 cm^{-1} corresponding to –OH stretching vibration became strong after sulfonation reaction. It further illustrated that CNTs was sulfonated successfully by concentrated sulfuric acid and obtained sCNTs. In the surface treatment process, the sulfate groups of concentrated sulfuric acid reacted with the unstable carbon atoms on the defect sites to generate –SO$_3$H groups on the surface of CNTs [30]. Figure 2 shows the TEM image of sulfonated CNTs. It could be observed that CNTs exhibited the homogeneous network structure. The string of CNTs had same diameter. The silk-like CNTs arranged together regularly, but they did not appear entanglement. It indicated that CNTs did not present self-aggregation due to the introduction of the hydrophilic –SO$_3$H groups onto surface of CNTs, and the sCNTs had more solubility than pristine CNTs as a result of the increase of surface polarity of CNTs.

Fabrication of PANI/NiHCF/sCNTs composite films

Figure 3 shows the cyclic voltammograms of PANI/NiHCF/sCNTs composite films during the electrodeposition at different concentration of NiSO$_4$ and K$_3$Fe(CN)$_6$. As shown in Fig. 3a, b, three pairs of redox characteristic peaks were obtained during the potential cycling scan. The first pair of peaks (around 0.24 and −0.004 V vs. SCE) is attributed to the redox reaction of PANI, namely to the reversible oxidation of leucoemarldine to emeraldine form. The second pair of peaks (around 0.44 and 0.27 V vs. SCE) is assigned to the redox reaction of NiHCF as the result of the change between Fe^{2+} to Fe^{3+} alternately. The third pair of peaks (around 0.74 and 0.59 V vs. SCE) is ascribed to the transformation from emeraldine to fully oxidized states for PANI. The peak current increased with the increase of the potential cycles apparently. As shown in Fig. 3c, d, only a pair of redox characteristic peaks e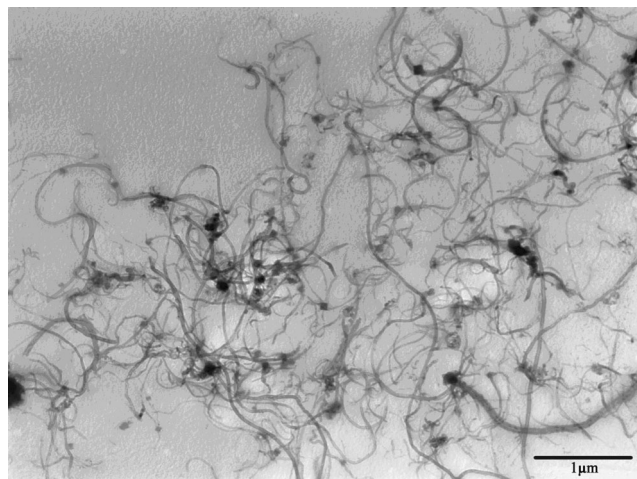xisted during the electrodeposition. It is attributed to the redox reaction of NiHCF, because electrodeposition of NiHCF played an important role with the increase of the concentration of NiSO$_4$ and K$_3$Fe(CN)$_6$ in the solution, whereas the electrodeposition of PANI decreased. In addition, it could be observed that the peak current of composite films increased with the increase of concentration of NiSO$_4$ and K$_3$Fe(CN)$_6$ in the prepared solution and the peak position shifted to positive. That demonstrated that the thickness of composite films increased linearly and the films had high electroactivity with increasing concentration of NiSO$_4$ and K$_3$Fe(CN)$_6$. This was because that the increase of electrodeposition amounts of NiHCF resulted in the increase of electrostatic attraction among the negatively charged metal hexacyanoferrate, negatively charged sCNTs and positively charge polyaniline (partially oxidized), leading to robust composite films. In addition, the degree of electron delocalization was accelerated by the π–π* electron interaction, which facilitated formation of electron transfer composites and improved conductivity [31].

Morphology of PANI/NiHCF/sCNT composite films

Figure 4 shows SEM images of PANI/NiHCF/sCNT composite films grown from various concentration of NiSO$_4$ and K$_3$Fe(CN)$_6$ in prepared solution. Distinct film structures were obtained as a result of the change of concentration of NiSO$_4$ and K$_3$Fe(CN)$_6$. As shown in Fig. 4a, the packing structure of short nanotubes with the diameter in the range from 0.23 to 0.30 μm was obtained in the prepared solution, which involved in 0.005 mol L^{-1} NiSO$_4$ and 0.005 mol L^{-1} K$_3$Fe(CN)$_6$, respectively. As presented in Fig. 4b, the short nanotubes changed into microparticles with the diameter in range from 0.30 to 0.40 μm with the concentration of 0.01 mol L^{-1} NiSO$_4$ and 0.01 mol L^{-1} K$_3$Fe(CN)$_6$. As shown in Fig. 4c, when the concentration of NiSO$_4$ and K$_3$Fe(CN)$_6$ increased to 0.02 mol L^{-1} NiSO$_4$ and 0.02 mol L^{-1} K$_3$Fe(CN)$_6$, respectively, the composite films formed the cubic particle structure, which were packed together, and the diameter of cubic particle was about 0.4–0.50 μm. As presented in Fig. 4d, the beautiful coral-like structure appeared as the concentration increased to 0.04 mol L^{-1} NiSO$_4$ and 0.04 mol L^{-1} K$_3$Fe(CN)$_6$, respectively, and the diameter of cubic particle in the coral-like structure was about 0.55–0.60 μm. It was noteworthy that the size of microparticles increased with the increase of concentration of NiSO$_4$ and K$_3$Fe(CN)$_6$. This indicated that electrodeposition rate of PANI/NiHCF/sCNT composite films increased and thickness increased obviously with the increase of concentration of solutions. The reason was that sCNTs in solution not only supplied high surface area and facilitated the charge transfer but also donated a large amount of proton to aniline polymerization and doping reaction to form more charge transfer composites. Therefore, the thickness and size of PANI/NiHCF/
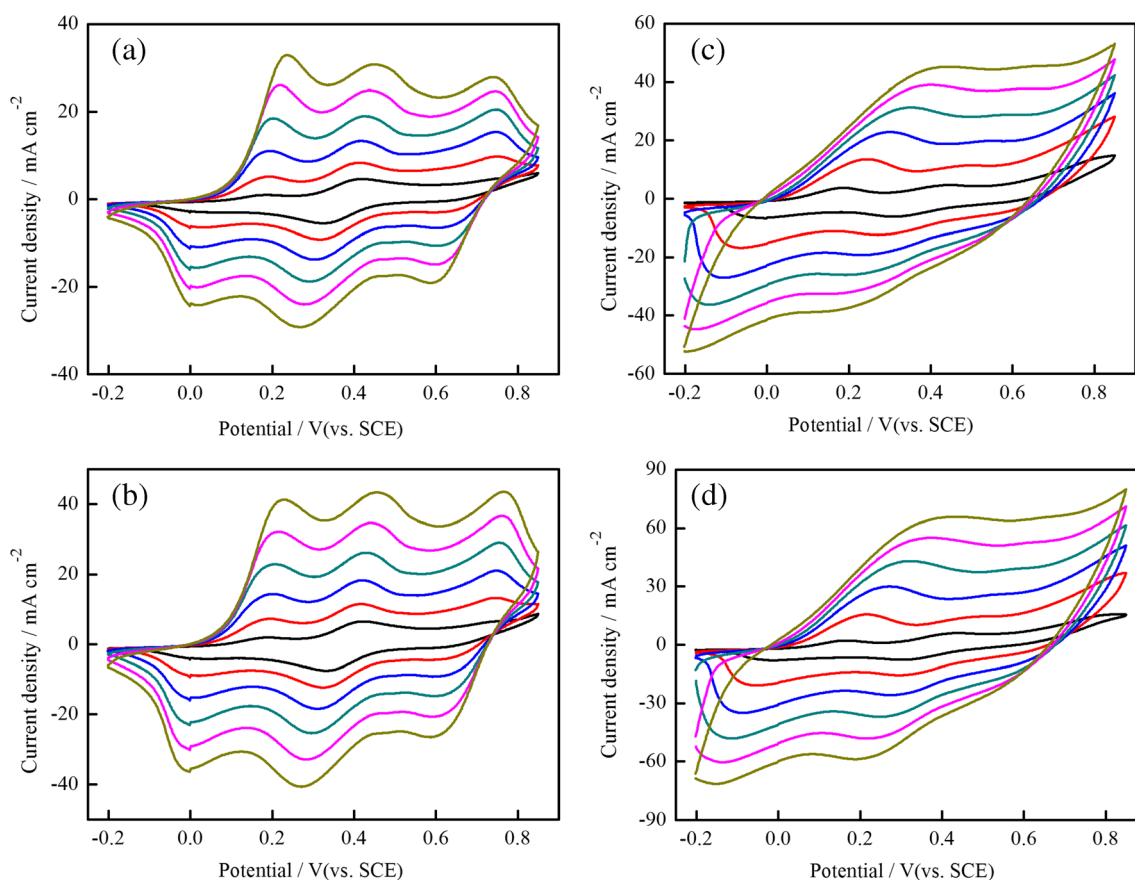

Fig. 2 TEM of sCNTs

Fig. 3 The cyclic voltammograms of PANI/NiHCF/sCNT composite films' electrodeposition on platinum electrode in the solution of sCNTs, NiSO$_4$, Na$_2$SO$_4$, K$_3$Fe(CN)$_6$, and aniline at different concentration of NiSO$_4$ and K$_3$Fe(CN)$_6$. The concentration of NiSO$_4$ and K$_3$Fe(CN)$_6$ in the solution was as follows: **a** 0.005 mol L^{-1}, **b** 0.01 mol L^{-1}, **c** 0.02 mol L^{-1}, and **d** 0.04 mol L^{-1}. *Scan rate 50 mV s^{-1}*

sCNT composite films increased with the increase of concentration of NiSO$_4$ and K$_3$Fe(CN)$_6$.

Figure 5 depicts the electrodeposition mechanism of PANI/NiHCF/sCNT composite films. A mixture of sCNTs, NiSO$_4$, Na$_2$SO$_4$, K$_3$Fe(CN)$_6$, and aniline formed stable aqueous dispersion as a result of introducing –SO$_3$H groups on the surface of sCNTs, which obtained good hydrophilicity. As shown in Fig. 5a, when the positive potential was applied during the initial cyclic voltametric scans, the negatively charged sCNTs were absorbed on the working electrode. A large amount of aniline molecules was adsorbed on the surface of sCNTs due to the π–π* electron interaction between aniline monomers and CNTs and hydrogen bonding interaction between the amino groups of aniline monomers and the –SO$_3$H groups of sCNTs [31–33]. Aniline monomers were polymerized to form oligomer and then formed long chain macromolecule on the surface of sCNTs and gaps between sCNTs, when the positive potential increased generally. The interconnected structure of PANI and sCNTs was formed, where PANI films coated on the surface of sCNTs and PANI molecular chains connected with sCNTs. Meanwhile, a large quantity of the negatively charged Fe(CN)$_6^{3-}$ was adsorbed on surface of

PANI coating sCNTs and PANI molecular chains in gaps between sCNTs due to the electrostatic attraction of the positively charged interconnected structure films and emeraldine state. As shown in Fig. 5b, when the negative potential was applied on the electrode, the Fe(CN)$_6^{3-}$ was reduced to Fe(CN)$_6^{4-}$ and instantaneously reacted with Ni^{2+} to yield NiHCF deposited on the surface of PANI coating sCNTs and PANI molecular chains, and then the cubic PANI/NiHCF microparticles were formed and piled on the PANI and sCNTs. More and more cubic PANI/NiHCF microparticles were distributed on the surface of electrode with increasing negative potential. Therefore, the cubic packing structure of PANI/NiHCF/sCNTs composite films was obtained with so many times cyclic voltammeric scans, which was agreement with the results of SEM image. Kulesza et al. [34] also reported that the PANI/NiHCF composite films were not a simple mixture of NiHCF and PANI as a result of the existence of electrostatic attraction between the negatively charged metal hexacyanoferrate and the positively charge polyaniline (partially oxidized). During electrodeposition by potential cycling scans alternate layers of PANI and NiHCF were produced. In our study, sulfonated carbon nanotubes are anionic, which
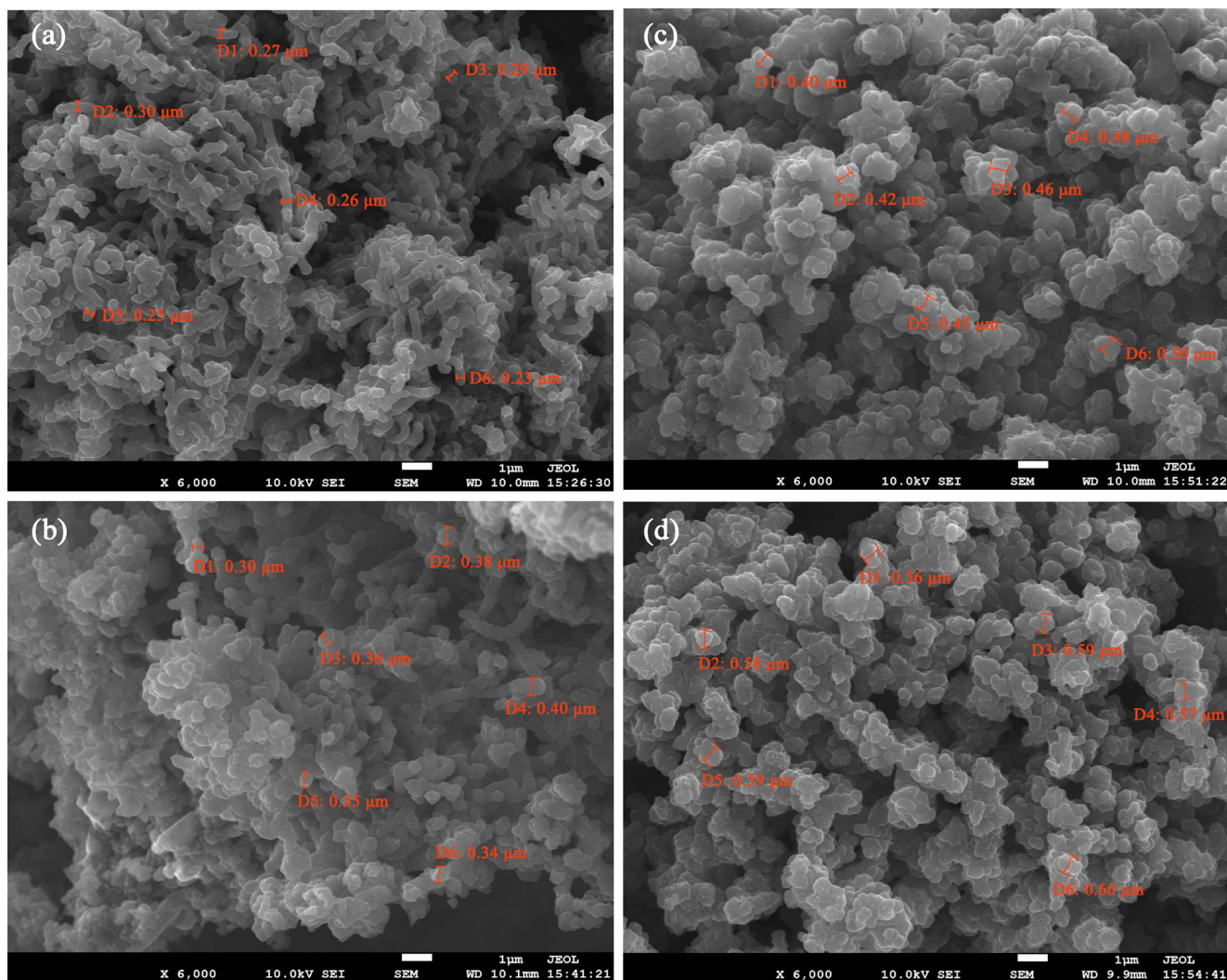
Fig. 4 SEM images of PANI/NiHCF/sCNT composite films grown on platinum substrate from various concentration of $NiSO_4$ and $K_3Fe(CN)_6$ in the prepared solutions. The concentration of $NiSO_4$ and $K_3Fe(CN)_6$ in the solution was as follows: **a** 0.005 mol L^{-1}, **b** 0.01 mol L^{-1}, **c** 0.02 mol L^{-1}, and **d** 0.04 mol L^{-1}

have the electrostatic attraction with positively charge PANI and could be absorbed on surface of electrode during positive potential scans.

Structural characterization of PANI/NiHCF/sCNT composite films

FTIR spectra

Figure 6 shows the FTIR spectra of PANI/NiHCF/sCNT composite films prepared from different concentration of $NiSO_4$ and $K_3Fe(CN)_6$. As shown in Fig. 6, the peaks at 3407 cm^{-1} are attributed to the NH stretching vibration in polyaniline. The absorption peaks at 2140 cm^{-1} are assigned to the CN stretching vibration in the Fe^{2+}–CN–Fe^{3+} of NiHCF. Compared with the peaks at 2090 cm^{-1} in NiHCF [35], there was a blue shift of the absorption of –CN– stretching vibrations,

indicating the existence of electrostatic attraction among PANI, NiHCF, and sCNTs. The bands at 1693 cm^{-1} are due to the C=C stretching vibration of benzene rings, while the absorption peaks at 1492 cm^{-1} are attributed to the C=C stretching vibration of the nitrogen quinine [36], and the peaks at 1292 and 1143 cm^{-1} are assigned to asymmetric and symmetric stretching of –SO_3H groups, which had slight increase in comparison with the absorption at 1460 and 1220 cm^{-1} in sCNTs, indicating a red shift of the absorption of –SO_3H groups occurred. This also demonstrated that the electrostatic attraction taken place during electrodeposition [26]. The bands at 994 cm^{-1} are assigned to SO_4^{2-} doped PANI [37]. The intensity of peaks at 2140 cm^{-1} increased with increasing concentration of $NiSO_4$ and $K_3Fe(CN)_6$, while the intensity of peaks at 3407 cm^{-1} decreased. This revealed that the amount of NiHCF deposited in composite films increased with increase of concentration of $NiSO_4$ and $K_3Fe(CN)_6$, but the

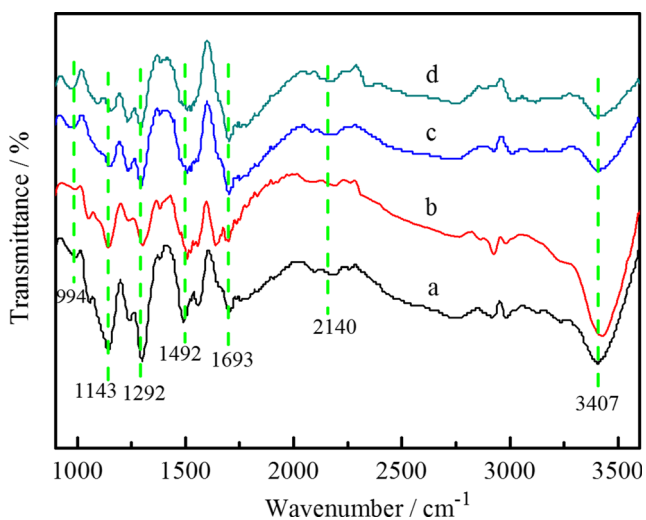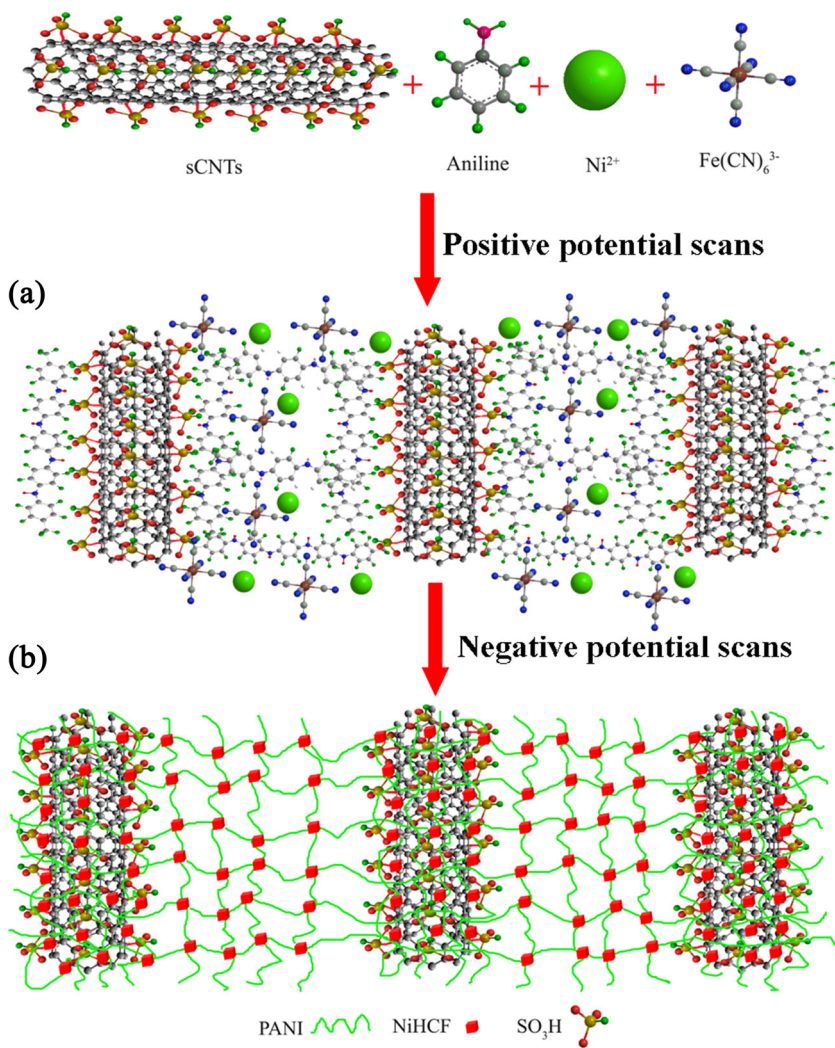**Fig. 5** Schematic illustration of the formation mechanism of PANI/NiHCF/sCNT composite films

Fig. 6 FTIR spectra of PANI/NiHCF/sCNT composite films prepared from different concentration of NiSO$_4$ and K$_3$Fe(CN)$_6$. The concentration of NiSO$_4$ and K$_3$Fe(CN)$_6$ in the solution was as follows: *a*, 0.005 mol L^{-1}; *b*, 0.01 mol L^{-1}; *c*, 0.02 mol L^{-1}; and *d* 0.04 mol L^{-1}

amount of PANI deposited decreased. Based on FTIR results, PANI, NiHCF, and sCNTs were deposited on the platinum electrode by potential cycling alternate and the electrostatic attraction existed among PANI, NiHCF, and sCNTs.

XRD analysis

Figure 7 shows XRD patterns of PANI/NiHCF/sCNT composite films prepared from different concentration of NiSO$_4$ and K$_3$Fe(CN)$_6$. As shown in Fig. 7, the crystalline peaks appear at $2\theta=25.6°$ and 29.7°, corresponding to the (200) and (022) crystal planes of PANI in its emeraldine salt form [38], respectively. The peaks around 40° are attributed to the (100) graphitic planes inside the walls of the sCNTs [39]. The peaks around 43.5° and 46.5° are due to the (422) and (200) crystal planes of nickel and platinum [40, 41], respectively. As an increase of concentration of NiSO$_4$ and K$_3$Fe(CN)$_6$, the intensity of characteristic bands of PANI decreased, while intensity of characteristic peaks of nickel increased. This demonstrated that PANI, NiHCF, and sCNTs are electrodeposited
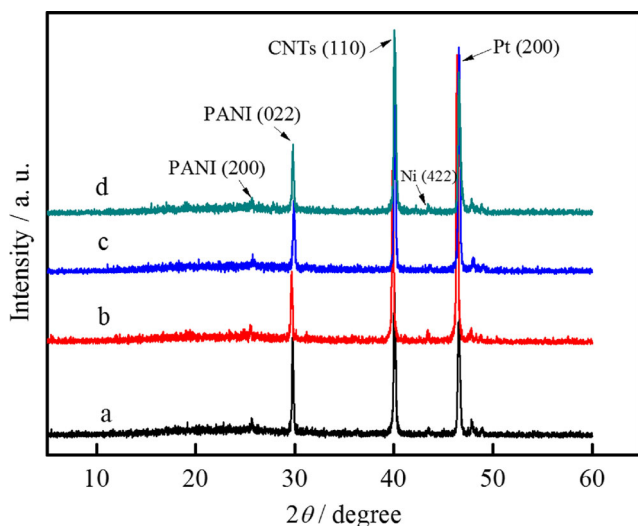
Fig. 7 Typical XRD patterns of PANI/NiHCF/sCNT composite films prepared from different concentration of NiSO$_4$ and K$_3$Fe(CN)$_6$. The concentration of NiSO$_4$ and K$_3$Fe(CN)$_6$ in the solution was as follows: *a*, 0.005 mol L^{-1}; *b*, 0.01 mol L^{-1}; *c*, 0.02 mol L^{-1}; *d*, 0.04 mol L^{-1}

on the platinum electrode by the one-step co-polymerization using cyclic voltammetry.

Electrochemical characterization

Electroactivity

Figure 8 shows the voltammetric responses of PANI/NiHCF/sCNT composite films recorded in 0.5 mol L^{-1} H$_2$SO$_4$ and 0.5 mol L^{-1} KNO$_3$ mixed solution. Composite films were prepared in solutions, which contained various concentration of NiSO$_4$ and K$_3$Fe(CN)$_6$, namely 0.005, 0.01, 0.02, and 0.04 mol L^{-1}, respectively. As shown in Fig. 8, the general features of composite films cyclic voltammetric peaks were
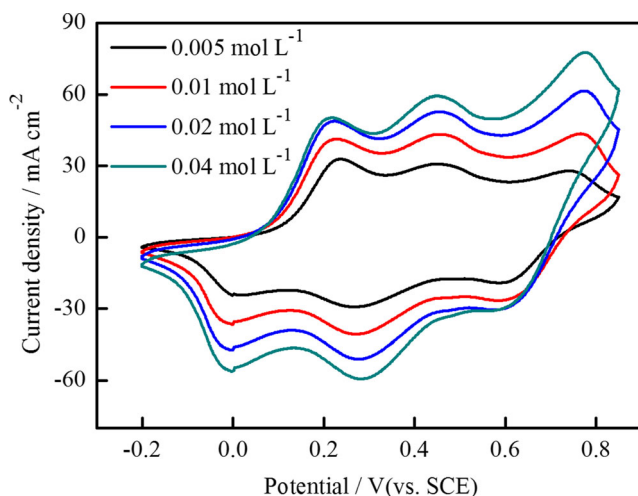

Fig. 8 The voltammetric responses of PANI/NiHCF/sCNT composite films prepared from different concentration of NiSO$_4$ and K$_3$Fe(CN)$_6$ recorded in 0.5 mol L^{-1} H$_2$SO$_4$ and 0.5 mol L^{-1} KNO$_3$ mixed solution. *Scan rate* 50 mV s^{-1}

agreement with previous report for PANI/NiHCF electrodes and have been discussed in detail [20–22, 42]. The anodic and cathodic redox peaks (ca. 0.20 and −0.005 V vs. SCE) are attributed to transformation from leucoemeraldine to emeraldine for PANI. The characteristic peaks (ca. 0.78 and 0.6 V vs. SCE) are assigned to transformation from emeraldine to pernigraniline. The peaks at ca. 0.45 and 0.29 V vs. SCE are due to redox state of NiHCF, which can absorb and release potassium cations during cycle potential [43], respectively. It was seen from Fig. 8 that peak current increased with the increase of concentration of NiSO$_4$ and K$_3$Fe(CN)$_6$ in the solution. Furthermore, the anodic and cathodic redox peaks shifted toward positive and negative, respectively. The results implied that composite films became highly robust and electroactive, which were prepared in high concentration. In addition, it can be demonstrated that PANI/NiHCF/sCNT composite films have the good pseudocapacitance characteristics except for double-layer capacitance performance originated from sCNTs.

EIS analysis

Figure 9 shows the EIS spectra of PANI/NiHCF/sCNT composite films prepared by different concentration of NiSO$_4$ and K$_3$Fe(CN)$_6$ recorded in 0.5 mol L^{-1} H$_2$SO$_4$ and 0.5 mol L^{-1} KNO$_3$ mixed solution. It can be seen that EIS spectra are almost similar, which include a distorted semicircle in the high-frequency region due to instinct characteristic of the electrode and a linear part at the low frequency end due to a diffusion-controlled doping and undoping of anions that results from Warburg behavior [44]. The diameter of semicircle is equal to the electron transfer resistance (R_{et}), which controls the electron transfer kinetics of the redox process at the electrode interface. R_{et} of composite films decreased with the increase of concentration of NiSO$_4$ and K$_3$Fe(CN)$_6$. As shown in Fig. 9a, the R_{et} was estimated to be about 360 and 223 Ω, when concentration of NiSO$_4$ and K$_3$Fe(CN)$_6$ was 0.005 and 0.01 mol L^{-1}, respectively. As shown in Fig. 9b, after concentration of NiSO$_4$ and K$_3$Fe(CN)$_6$ increased to 0.02 and 0.04 mol L^{-1}, respectively, the R_{et} decreases dramatically to about 9.9 and 5.9 Ω. This implied that more and more the large size of microparticles were distributed in PANI matrix and absorbed on surface of CNTs with increasing concentration of NiSO$_4$ and K$_3$Fe(CN)$_6$, the distance between NiHCF redox sites was reduced in the PANI matrix so that charge and electron were easy to be fast transferred in the interconnected network structure.

Galvanostatic charge/discharge characteristics

Figure 10 shows constant current charging/discharging curves of PANI/NiHCF/sCNT composite films prepared by different concentration of NiSO$_4$ and K$_3$Fe(CN)$_6$ recorded in 1 mol L^{-1}

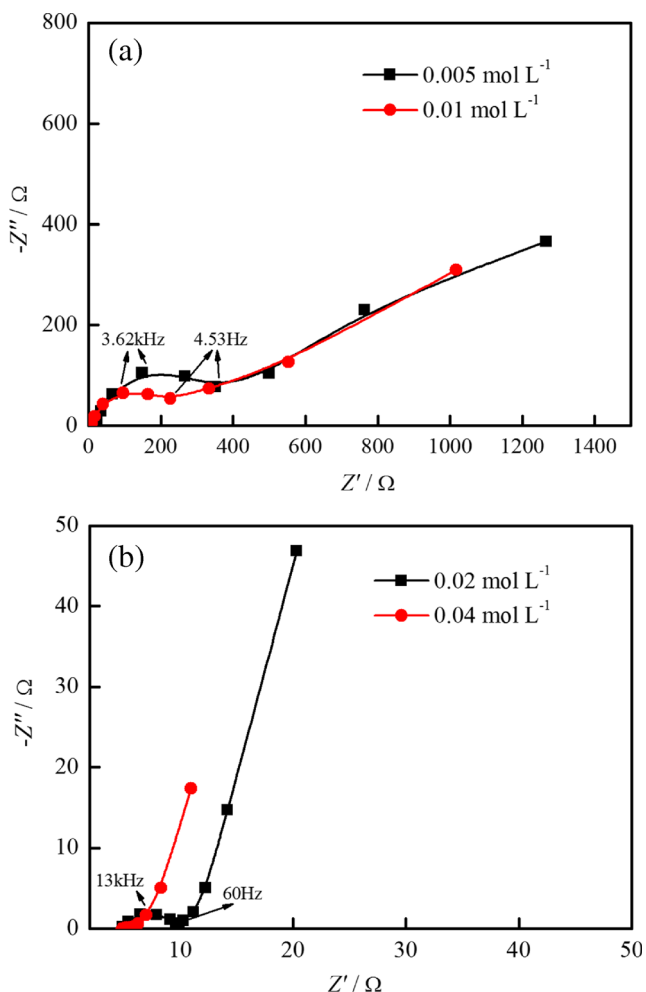Fig. 9 EIS spectra of PANI/NiHCF/sCNT composite films prepared from different concentration of NiSO$_4$ and K$_3$Fe(CN)$_6$ in 0.5 mol L^{-1} H$_2$SO$_4$ and 0.5 mol L^{-1} KNO$_3$. E 0.0 V, frequency range 100 kHz–0.1 Hz, amplitude 10 mV

Fig. 11 Specific capacitance of PANI/NiHCF/sCNT composite films prepared from different concentration of NiSO$_4$ and K$_3$Fe(CN)$_6$ recorded at a current density of 2 mA cm^{-2}

KNO$_3$ electrolyte at a current density of 2 mA cm^{-2} in the range of 0–0.7 V. As shown in Fig. 10, the potential changed with the time as a result of good capacitance of composite films. The discharge course had a sudden voltage drop due to the internal resistance of the composites films. But, this did not affect supercapacitive and energy storage properties [45]. The discharging course of composite films electrode was not ideal straight line and exhibits two voltage stages in the potential ranges of 0.70 to 0.40 V and 0.40 to 0 V (vs. SCE). The first stage was only contributed by ions separation in the electric double-layer region at both electrode interfaces [45], whereas the second stage was attributed to the combination of electric double-layer capacitance of sCNTs and pseudocapacitance of PANI and NiHCF [38]. On the basis of the galvanostatic charge/discharge curves, the specific
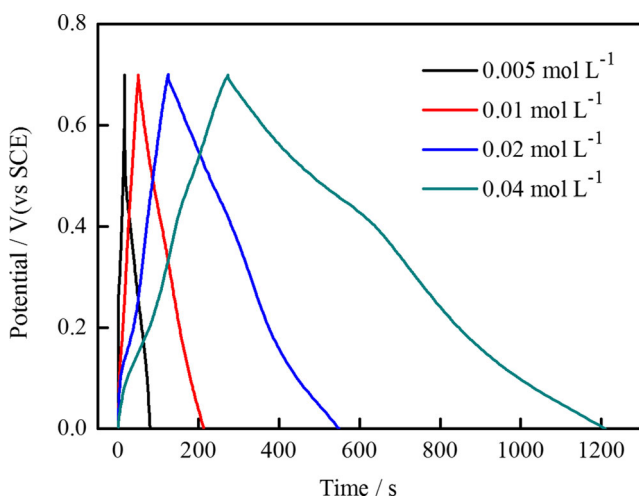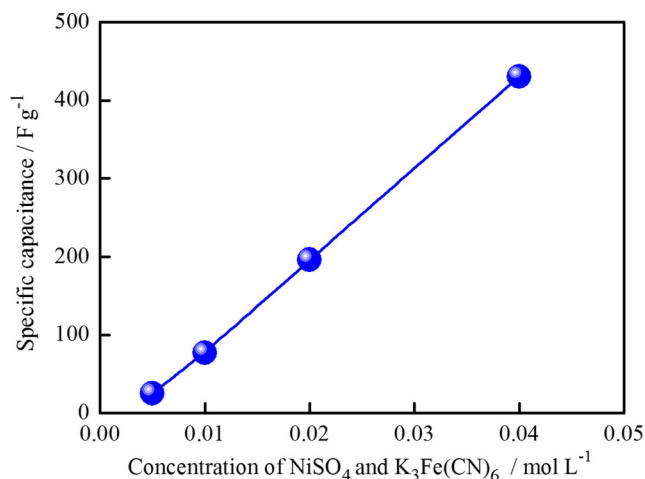

Fig. 10 Constant current charging/discharging curves of PANI/NiHCF/sCNT composite films prepared from different concentration of NiSO$_4$ and K$_3$Fe(CN)$_6$ recorded at a current density of 2 mA cm^{-2}
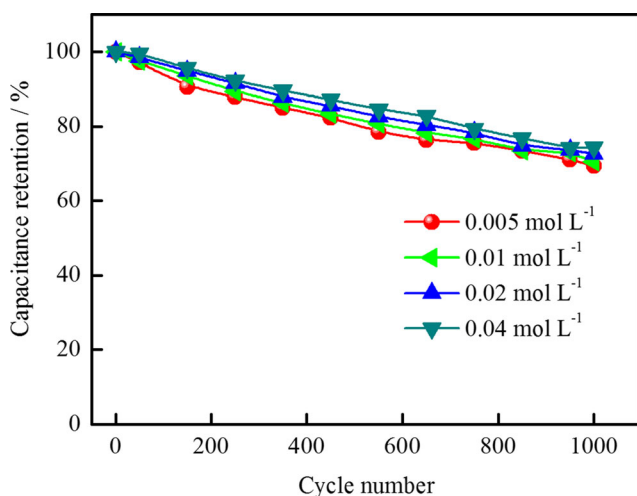

Fig. 12 Variation of the specific capacitance of PANI/NiHCF/sCNT composite films prepared from different concentration of NiSO$_4$ and K$_3$Fe(CN)$_6$ as a function of cycle number measured at a current density of 2 mA cm^{-2}

capacitance of PANI/NiHCF/sCNT composite films was calculated according to the following formula [46]:

$$C = \frac{I \Delta t}{m \Delta V} \quad (1)$$

where C is the specific capacitance, Δt is discharged time, m is the mass of the electrochemical materials on the current collector, ΔV is voltage range, and I is the charge/discharge current. Figure 11 shows the specific capacitance of PANI/NiHCF/sCNT composite films prepared by different concentration of $NiSO_4$ and $K_3Fe(CN)_6$. The specific capacitance of composite films increased linearly with increasing concentration of $NiSO_4$ and $K_3Fe(CN)_6$, and the highest specific capacitance of PANI/NiHCF/sCNT composite film being prepared in solution containing 0.04 mol L^{-1} $NiSO_4$ and 0.04 mol L^{-1} $K_3Fe(CN)_6$ was 430.77 F g^{-1}. This indicated that the capacitance performance was improved by synergistic effect of sCNTs and PANI. The reason was that sCNTs and NiHCF interacted strongly with the PANI via π–π^* electron stacking, which may facilitate more charge transfer and increased electron delocalization degree of the composites [31]. On the other hand, PANI could form the interconnected packing structure via NiHCF connection, which could transfer proton from one PANI phase to another PANI. As a result, the more concentration of $NiSO_4$ and $K_3Fe(CN)_6$ was, the higher capacitance performance was obtained. It was surprised that specific capacitance of composite films decreased sharply, when the concentration of $NiSO_4$ and $K_3Fe(CN)_6$ was more than 0.04 mol L^{-1} $K_3Fe(CN)_6$. This demonstrated that too much NiHCF were formed, resulting in stability decrease of the composite films. Furthermore, it was not beneficial to synergetic effect of composite films.

Cycle stability

Figure 12 shows the charge/discharge stability of PANI/NiHCF/sCNT composite films prepared from different concentration of $NiSO_4$ and $K_3Fe(CN)_6$ in 1 mol L^{-1} KNO_3 electrolyte at a current density of 2 mA cm^{-2} in the range of 0–0.7 V. As shown in Fig. 12, the capacitance retention of the composite films decreased with the cycle, whereas the capacitance retention obviously increased with the increase of concentration of $NiSO_4$ and $K_3Fe(CN)_6$ during 1000 cycles charge/discharge. When the concentration of $NiSO_4$ and $K_3Fe(CN)_6$ was 0.005, 0.01, 0.02, and 0.04 mol L^{-1}, the retention of the composite films was 69.43, 70.46, 72.57, and 74.33 % after 1000 cycles, respectively. These results revealed that the more NiHCF were produced, the more cycle stability of composite films was. The enhanced cycle stability of the composite films was attributed to existence of a large sum of –SO_3H groups in sCNTs, which can function as a large molecular dopant which was integrated and essentially locked to the PANI chains that ensured stability of the desired electrochemical properties. This prevented PANI molecular chains from swelling and shrinking during the long-term charge/discharge process. On the other hand, as the increase of the concentration of $NiSO_4$ and $K_3Fe(CN)_6$, more and more electron transfer composites with high stability were formed due to strong electrostatic interaction among sCNTs, PANI, and NiHCF.

Conclusions

PANI/NiHCF/sCNT interconnected composite films was fabricated successfully by the one step co-polymerization using cyclic voltammetry in the solution of sCNTs, $NiSO_4$, Na_2SO_4, $K_3Fe(CN)_6$, and aniline. The morphology, constant current charging/discharging, and electrochemical impedance of composite films were influenced by the concentration of $NiSO_4$ and $K_3Fe(CN)_6$ when other condition did not change. The sCNTs had uniform dispersibility due to the presence of sulfonic acid groups, which can supply the proton for PANI to perform doping/undoping reaction. With increasing concentration of $NiSO_4$ and $K_3Fe(CN)_6$, morphology of PANI/NiHCF/sCNTs composite film changed from the short nanotubes to microparticle and coral-like structure as a result of the π–π^* electron, and hydrogen bonding interaction among sCNTs, NiHCF, and PANI. The supercapacitive performance increased with the increase of concentration of $NiSO_4$ and $K_3Fe(CN)_6$. The electron transfer resistance reduced to 5.9 Ω from 360 Ω, and specific capacitance increased to 430.77 F g^{-1} from 25 F g^{-1}, when concentration of $NiSO_4$ and $K_3Fe(CN)_6$ changed from 0.005 mol L^{-1} to 0.04 mol L^{-1}. The cycle stability of the composite films increased with the increase of concentration of $NiSO_4$ and $K_3Fe(CN)_6$, which was ascribed to existence of a large sum of –SO_3H groups in sCNTs and strong electrostatic interaction sCNTs, PANI, and NiHCF.

References

1. Wang HL, Hao QL, Yang XJ, Lu LD, Wang X (2009) Graphene oxide doped polyaniline for supercapacitors. Electrochem Commun 11:1158–1161
2. Frackowiak E, Béguin F (2001) Carbon materials for the electrochemical storage of energy in capacitors. Carbon 39:937–950
3. Kötz R, Carlen M (2000) Principles and applications of electrochemical capacitors. Electrochim Acta 45:2483–2498

4. Malak A, Fic K, Lota G, Vix-Guterl C, Frackowiak E (2010) Hybrid materials for supercapacitor application. J Solid State Electr 14:811–816

5. Yang MM, Cheng B, Song HH, Chen XH (2010) Preparation and electrochemical performance of polyaniline-based carbon nanotubes as electrode material for supercapacitor. Electrochim Acta 55:7021–7027

6. Qu DY, Shi H (1998) Studies of activated carbons used in double-layer capacitors. J Power Sources 74:99–107

7. Zhang Y, Feng H, Wu XB, Wang LZ, Zhang AQ, Xia TC, Dong HC, Li XF, Zhang LS (2009) Progress of electrochemical capacitor electrode materials: a review. Int J Hydrogen Energ 34:4889–4899

8. Wang GP, Zhang L, Zhang JJ (2012) A review of electrode materials for electrochemical supercapacitors. Chem Soc Rev 41:797–828

9. Ji HX, Zhao X, Qiao ZH, Jung J, Zhu YW, Lu YL, Zhang LL, MacDonald AH, Ruoff RS (2014) Capacitance of carbon-based electrical double-layer capacitors. Nat Commun 5:1–7

10. Ryu KS, Kim KM, Park NG, Park YJ, Chang SH (2002) Symmetric redox supercapacitor with conducting polyaniline electrodes. J Power Sources 103:305–309

11. Fu QB, Gao B, Dou H, Hao L, Lu XJ, Sun K, Jiang JC, Zhang XG (2011) Novel non-covalent sulfonated multiwalled carbon nanotubes from p-toluenesulfonic acid/glucose doped polypyrrole for electrochemical capacitors. Synthetic Met 161:373–378

12. Zhi MJ, Xiang CC, Li JT, Li M, Wu NQ (2013) Nanostructured carbon-metal oxide composite electrodes for supercapacitors: a review. Nanoscale 5:72–88

13. Li D, Huang JX, Kaner RB (2008) Polyaniline nanofibers: a unique polymer nanostructure for versatile applications. Accounts Chem Res 42:135–145

14. Jiang HF, Liu XX (2010) One-dimensional growth and electrochemical properties of polyaniline deposited by a pulse potentiostatic method. Electrochim Acta 55:7175–7181

15. Iijima S, Ichihashi T (1993) Single-shell carbon nanotubes of 1-nm diameter. Nature 363:603–605

16. Niu CM, Sichel EK, Hoch R, Moy D, Tennent H (1997) High power electrochemical capacitors based on carbon nanotube electrodes. Appl Phys Lett 70:1480–1482

17. Malik MA, Miecznikowski K, Kulesza PJ (2000) Quartz crystal microbalance monitoring of mass transport during redox processes of cyanometallate modified electrodes: complex charge transport in nickel hexacyanoferrate films. Electrochim Acta 45:3777–3784

18. Bácskai J, Martinusz K, Czirók E, Inzelt G, Kulesza PJ, Malik MA (1995) Polynuclear nickel hexacyanoferrates: monitoring of film growth and hydrated counter-cation flux/storage during redox reactions. J Electroanal Chem 385:241–248

19. Lin YH, Cui XL (2006) Electrosynthesis, characterization, and application of novel hybrid materials based on carbon nanotube-polyaniline-nickel hexacyanoferrate nanocomposites. J Mater Chem 16:585–592

20. Wang YH, Yang YJ, Hao XG, Zhang XR, Zhang ZL, Ma GZ (2014) pH-controlled morphological structure and electrochemical performances of polyaniline/nickel hexacyanoferrate nanogranules during electrochemical deposition. J Solid State Electr 18:2885–2892

21. Zang Y, Hao XG, Wang ZD, Zhang ZL, Liu SB (2010) Copolymerization and capacitive performance of composite carbon nanotubes/polyaniline/nickel hexacyanoferrate films. Acta Phys-Chim Sin 26:291–298

22. Li XM, Du X, Wang ZD, Hao XG, Guan GQ, Zhang H, Abuliti A, Ma GZ (2014) Electroactive NiHCF/PANI hybrid films prepared by pulse potentiostatic method and its performance for H_2O_2 detection. J Electroanal Chem 717–718:69–77

23. Peng F, Zhang L, Wang HJ, Lv P, Yu H (2005) Sulfonated carbon nanotubes as a strong protonic acid catalyst. Carbon 43:2405–2408

24. Wang HJ, Yu H, Peng F, Lv P (2006) Methanol electrocatalytic oxidation on highly dispersed Pt/sulfonated-carbon nanotubes catalysts. Electrochem Commun 8:499–504

25. Hudson JL, Casavant MJ, Tour JM (2004) Water-soluble, exfoliated, nonroping single-wall carbon nanotubes. J Am Chem Soc 126:11158–11159

26. Yu H, Jin YG, Li Z, Peng F, Wang HJ (2008) Synthesis and characterization of sulfonated single-walled carbon nanotubes and their performance as solid acid catalyst. J Solid State Chem 181:432–438

27. Peng C, Jin J, Chen GZ (2007) A comparative study on electrochemical co-deposition and capacitance of composite films of conducting polymers and carbon nanotubes. Electrochim Acta 53:525–537

28. Wei ZX, Wan MX, Lin T, Dai L (2003) Polyaniline nanotubes doped with sulfonated carbon nanotubes made via a self-assembly process. Adv Mater 15:136–139

29. Wang YB, Iqbal Z, Mitra S (2005) Rapidly functionalized, water-dispersed carbon nanotubes at high concentration. J Am Chem Soc 128:95–99

30. Choudhury A, Kar P (2011) Doping effect of carboxylic acid group functionalized multi-walled carbon nanotube on polyaniline. Compos Part B-Eng 42:1641–1647

31. Zhu ZZ, Wang GC, Sun MQ, Li XW, Li CZ (2011) Fabrication and electrochemical characterization of polyaniline nanorods modified with sulfonated carbon nanotubes for supercapacitor applications. Electrochim Acta 56:1366–1372

32. Chaudhari HK, Kelkar DS (1997) Investigation of structure and electrical conductivity in doped polyaniline. Polym Int 42:380–384

33. Wu TM, Lin YW, Liao CS (2005) Preparation and characterization of polyaniline/multi-walled carbon nanotube composites. Carbon 43:734–740

34. Kulesza PJ, Miecznikowski K, Malik MA, Galkowski M, Chojak M, Caban K, Wieckowski A (2001) Electrochemical preparation and characterization of hybrid films composed of Prussian blue type metal hexacyanoferrate and conducting polymer. Electrochim Acta 46:4065–4073

35. Zou YJ, Sun LX, Xu F (2007) Biosensor based on polyaniline-prussian blue/multi-walled carbon nanotubes hybrid composites. Biosens Bioelectron 22:2669–2674

36. Boruah M, Kalita A, Pokhrel B, Dolui SK, Boruah R (2013) Synthesis and characterization of pH responsive conductive composites of poly(acrylic acid-co-acrylamide) impregnated with polyaniline by interfacial polymerization. Adv Polym Tech 32:E520–E530

37. Bogdanović U, Vodnik VV, Ahrenkiel SP, Stoiljković M, Ćirić-Marjanović G, Nedeljković JM (2014) Interfacial synthesis and characterization of gold/polyaniline nanocomposites. Synthetic Met 195:122–131

38. Yan J, Wei T, Fan ZJ, Qian WZ, Zhang ML, Shen XD, Wei F (2010) Preparation of graphene nanosheet/carbon nanotube/polyaniline composite as electrode material for supercapacitors. J Power Sources 195:3041–3045

39. Saini P, Choudhary V, Singh BP, Mathur RB, Dhawan SK (2009) Polyaniline-MWCNT nanocomposites for microwave absorption and EMI shielding. Mater Chem Phys 113:919–926

40. Mimura H, Lehto J, Harjula R (1997) Chemical and thermal stability of potassium nickel hexacyanoferrate (II). J Nucl Sci Technol 34:582–587

41. Shi J, Guo DJ, Wang Z, Li HL (2005) Electrocatalytic oxidation of formic acid on platinum particles dispersed in SWNT/PANI composite film. J Solid State Electr 9:634–638

42. Wang ZD, Sun SB, Hao XG, Ma XL, Guan GQ, Zhang ZL, Liu SB (2012) A facile electrosynthesis method for the controllable preparation of electroactive nickel hexacyanoferrate/

polyaniline hybrid films for H_2O_2 detection. Sensor Actuat B-chem 171:1073–1080

43. Zamponi S, Berrettoni M, Kulesza PJ, Miecznikowski K, Malik MA, Makowski O, Marassi R (2003) Influence of experimental conditions on electrochemical behavior of Prussian blue type nickel hexacyanoferrate film. Electrochim Acta 48:4261–4269

44. Sun MQ, Wang GC, Li XW, Cheng QL, Li CZ (2012) Interfacial synthesis and supercapacitive performance of hierarchical sulfonated carbon nanotubes/polyaniline nanocomposites. Ind Eng Chem Res 51:3981–3987

45. Yu N, Gao L (2009) Electrodeposited PbO_2 thin film on Ti electrode for application in hybrid supercapacitor. Electrochem Commun 11:220–222

46. Wang Q, Yan J, Fan ZJ, Wei T, Zhang M, Jing XY (2014) Mesoporous polyaniline film on ultra-thin graphene sheets for high performance supercapacitors. J Power Sources 247:197–203